αS, were obtained from P. T. Lansbury [J. C. Rochet *et al.*, *Biochemistry* **39**, 10619 (2000)].
21. The silver-stained band at 22 kD in an HP2A immunoprecipitate of normal human brain and a co-migrating silver-negative slice from an adjacent lane of a parkin-preabsorbed HP2A precipitate were excised, trypsin digested and subjected to blind analysis by mass spectrometry at MDS Proteomics, Inc. (Toronto, ON) [A. Shevchenko *et al.*, *Anal. Chem.* **68**, 850 (1996)]. The HP2A-specific 22-kD protein yielded tryptic peptides corresponding to aa 13–21, 44–58, 46–58, 59–80, 61–80, 81–96, and 81–97 of human αS (GenBank accession # L08850), each ending with a lysine, as expected. No αS sequence was detected in the co-migrating slice from the preabsorbed lane.
22. Y. Mizuno, N. Hattori, H. Mori, *Biomed. Pharmacother.* **53**, 109 (1999).
23. H. Shimura *et al.*, *Ann. Neurol.* **45**, 668 (1999).
24. N. Hattori *et al.*, *Ann. Neurol.* **44**, 935 (1998).
25. A. L. Talis, J. M. Huibregtse, P. M. Howley, *J. Biol. Chem.* **273**, 6439 (1998).
26. M. Scheffner, J. M. Huibregtse, R. D. Vierstra, P. M. Howley, *Cell* **75**, 495 (1993).
27. Y. Jiang, E. Lev-Lehman, J. Bressler, T. F. Tsai, A. L. Beaudet, *Am. J. Hum. Genet.* **65**, 1 (1999).
28. Human UbcH7 and UbcH8 were expressed in M15 *E. coli* harboring the *Lac*-repressor expressing plasmid pREP4, using the QIA express system (QIAGEN, Valencia, CA) with an NH_2-terminal 6xHis tag. Proteins were purified on nickel NTA-agarose (QIAGEN). Enzymatic activity was tested in Ub shift assays.
29. Parkin was immunoprecipitated (yielding IP-parkin) from frontal cortex homogenates or HEK293 cells transiently transfected with myc-parkin cDNA (10 μg) (*13*). IP parkin was incubated at 37 °C in 50 μl of reaction buffer containing ATP (4 mM ATP in 50 mM Tris-HCl, pH 7.5, 2 mM $MgCl_2$), 100 ng of recombinant human E1, 2 μg of UbcH7 (E2), and 2 μg His-Ub (all from Affinity Research Products, Exeter, UK). The reaction was terminated by adding 20 μl of 4X sample buffer, and 25 μl aliquots of the reaction mixtures were electrophoresed and immunoblotted.
30. We prepared WT and ARPD-mutant parkin cDNAs [N. Hattori *et al.*, *Biochem. Biophys. Res. Commun.* **249**, 754 (1998); L. Terreni *et al.*, *Neurology* **56**, 463 (2001)] in a pcDNA3.1(+) vector using the QuikChange site-directed mutagenesis kit (Stratagene, La Jolla, CA) and transiently transfected them into HEK293 cells using Lipofectamine 2000 (Gibco, Rockville, MD), as per manufacturers' instructions.
31. For enzymatic digestion of HP2A precipitates, *N*-glycosidase, sialidase A, endo-*O*-glycosidase [with bovine fetuin as a control protein (ProZyme, San Leandro, CA)], and protein phosphatase-1 (Sigma) were used as per manufacturers' instructions.
32. C. A. Joazeiro, A. M. Weissman, *Cell* **102**, 549 (2000).
33. P. J. Kahle *et al.*, *J. Neurosci.* **20**, 6365 (2000).
34. M. Ivan *et al.*, *Science* **292**, 464 (2001).
35. P. Jaakkola *et al.*, *Science* **292**, 468 (2001).
36. J. Q. Trojanowski, M. Goedert, T. Iwatsubo, V. M. Lee, *Cell Death Differ.* **5**, 823 (1999).
37. M. S. Goldberg, P. T. Lansbury, *Nature Cell Biol.* **2**, E115 (2000).
38. N. F. Bence, R. M. Sampat, R. R. Kopito, *Science* **292**, 1552 (2001).
39. C. J. Cummings *et al.*, *Neuron* **24**, 879 (1999).
40. L. Wells, K. Vosseller, G. W. Hart, *Science* **291**, 2376 (2001).
41. We thank H. Mori, Y. Mizutani, and K. Yamane for ARPD brain specimens; J. Chan for providing normal human brain; and the patients' families for the donation of tissue. We also thank K. Wynn and P. Howley for anti-E6-AP (JH-16), T. Suzuki and K. Tanaka for a parkin cDNA-containing vector, P. Lansbury for reagents and critical review of our manuscript, and M. Medina for experimental advice. H.S. is supported by a Pergolide Fellowship (Eli Lilly, Japan K.K.). M.G.S. is supported by the Grass Foundation (Robert S. Morison Fellowship), the Lefler Foundation, and the NIH (NS 02127). M.P.F. is supported by a Beeson Scholar Award. R.S. received grants from the National Bank of Austria. Supported by the Morris R. Udall Center of Excellence in PD (NS 38375) at Brigham and Women's Hospital (M.P.F., K.S.K., and D.J.S.).

12 March 2001; accepted 6 June 2001
Published online 28 June 2001;
10.1126/science.1060627
Include this information when citing this paper.

REPORTS

Visible-Light Photocatalysis in Nitrogen-Doped Titanium Oxides

R. Asahi,* T. Morikawa, T. Ohwaki, K. Aoki, Y. Taga

To use solar irradiation or interior lighting efficiently, we sought a photocatalyst with high reactivity under visible light. Films and powders of $TiO_{2-x}N_x$ have revealed an improvement over titanium dioxide (TiO_2) under visible light (wavelength < 500 nanometers) in optical absorption and photocatalytic activity such as photodegradations of methylene blue and gaseous acetaldehyde and hydrophilicity of the film surface. Nitrogen doped into substitutional sites of TiO_2 has proven to be indispensable for band-gap narrowing and photocatalytic activity, as assessed by first-principles calculations and x-ray photoemission spectroscopy.

Since photoinduced decomposition of water on TiO_2 electrodes was discovered (*1*), semiconductor-based photocatalysis has attracted extensive interest. One particular focus has been on applications in which organic molecules are photodegraded, such as water and air purifications (*2–4*). Most of the investigations have focused on TiO_2 (*5–7*), which shows relatively high reactivity and chemical stability under ultraviolet (UV) light [wavelength (λ) < 387 nm], whose energy exceeds the band gap of 3.2 eV in the anatase crystalline phase.

The development of photocatalysts that can yield high reactivity under visible light (λ > 380 nm) should allow the main part of the solar spectrum, and even poor illumination of interior lighting, to be used. One approach has been to dope transition metals into TiO_2 (*8–10*), and another has been to form reduced TiO_x photocatalysts (*11*, *12*). However, doped materials suffer from a thermal instability (*9*), an increase of carrier-recombination centers, or the requirement of an expensive ion-implantation facility (*10*). Reducing TiO_2 introduces localized oxygen vacancy states located at 0.75 to 1.18 eV below the conduction band minimum (CBM) of TiO_2 (*12*), so that the energy levels of the optically excited electrons will be lower than the redox potential of the hydrogen evolution (H_2/H_2O) located just below the CBM of TiO_2 (*13*) and that the electron mobility in the bulk region will be small because of the localization.

We have considered whether visible-light activity could be introduced in TiO_2 by doping, and we set the following requirements: (i) doping should produce states in the band gap of TiO_2 that absorb visible light; (ii) the CBM, including subsequent impurity states, should be as high as that of TiO_2 or higher than the H_2/H_2O level to ensure its photoreduction activity; and (iii) the states in the gap should overlap sufficiently with the band states of TiO_2 to transfer photoexcited carriers to reactive sites at the catalyst surface within their lifetime. Conditions ii and iii require that we use anionic species for the doping rather than cationic metals, which often give quite localized *d* states deep in the band gap of TiO_2 and result in recombination centers of carriers. We have calculated densities of states (DOSs) of the substitutional doping of C, N, F, P, or S for O in the anatase TiO_2 crystal, by the full-potential linearized augmented plane wave (FLAPW) formalism (*14*, *15*) in the framework of the local density approximation (LDA) (*16*) (Fig. 1). The substitutional doping of N was the most effective because its *p* states contribute to the band-gap narrowing by mixing with O 2*p* states. Although doping with S shows a similar band-gap narrowing, it would be difficult to incorporate it into the TiO_2 crystal because of its large ionic radius, as evidenced by a much larger formation energy required for the substitution of S than that required for the substitution of N (*17*). The states introduced by C and P are too deep in the gap to satisfy condition iii. The calculated imaginary parts of the dielectric functions of $TiO_{2-x}N_x$ indeed show a shift of the absorption edge to a lower energy by the N doping (Fig. 2A) (*18*). Dominant transitions at the absorption edge have been identified with

Toyota Central R&D Laboratories, Nagakute, Aichi 480-1192, Japan.

*To whom correspondence should be addressed. E-mail: rasahi@mosk.tytlabs.co.jp

those from N $2p_\pi$ to Ti d_{xy}, instead of from O $2p_\pi$ as in TiO_2 (*19*). Jansen and Letschert demonstrated tunable colorings in modified perovskite oxinitrides, which suggested a similar band-gap control by N, although they did not address the detailed electronic states in these pigments (*20*).

Photocatalysts for the present purpose, however, require more elaborate controls for doping besides the optical absorption; i.e., conditions ii and iii. To this end, we have made a theoretical comparison among three systems: substitutional N doping, interstitial N doping, and both types of doping in the anatase TiO_2. In optimizing the positions of N in the eight TiO_2 units per cell, we observed molecularly bonding states—NO and N_2—for the last two cases; the obtained bond lengths of N–O and N–N were 1.20 and 1.16 Å, respectively, which are compared with those of the NO molecule (1.15 Å) and the N_2 molecule (1.10 Å). Such molecularly existing dopants give rise to the bonding states below the O 2*p* valence bands and antibonding states deep in the band gap (Fig. 1B, N_i and N_{i+s}). However, these states are well screened and hardly interact with the band states of TiO_2, and thus are unlikely to be effective for photocatalysis because of condition iii. The importance of substitutional site N doping is emphasized in the experimental results discussed below.

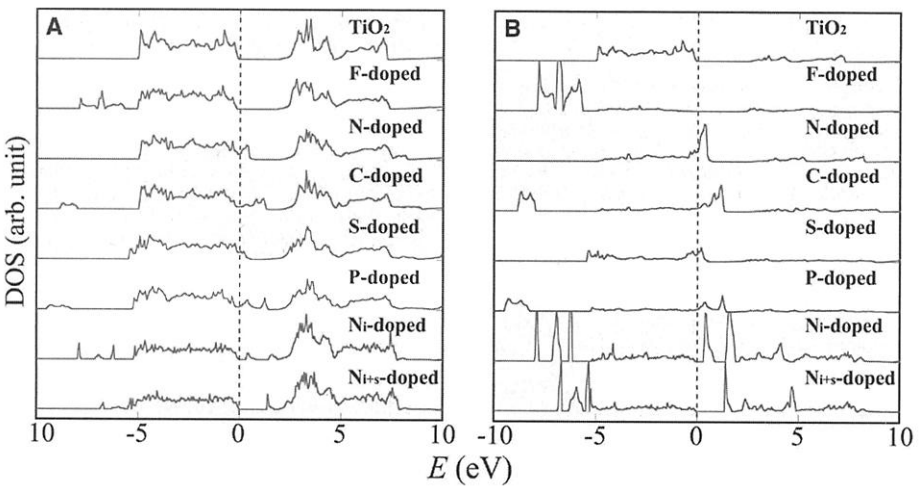

Fig. 1. (**A**) Total DOSs of doped TiO_2 and (**B**) the projected DOSs into the doped anion sites, calculated by FLAPW. The dopants F, N, C, S, and P were located at a substitutional site for an O atom in the anatase TiO_2 crystal (the eight TiO_2 units per cell). The results for N doping at an interstitial site (N_i-doped) and that at both substitutional and interstitial sites (N_{i+s}-doped) are also shown. The energy is measured from the top of the valence bands of TiO_2, and the DOSs for doped TiO_2 are shifted so that the peaks of the O 2*s* states (at the farthest site from the dopant) are aligned with each other. Arb. unit, arbitrary units.

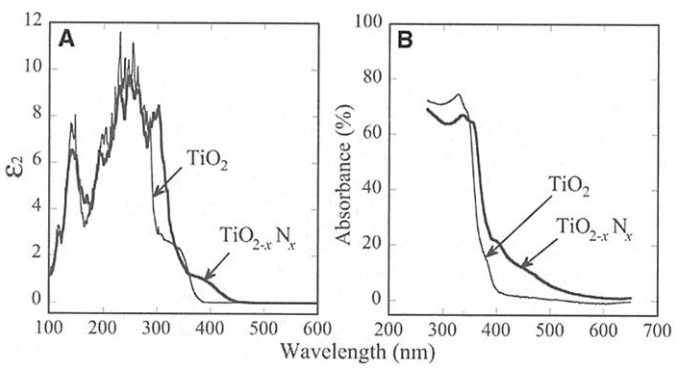

Fig. 2. Optical properties of $TiO_{2-x}N_x$ (thick lines) compared with TiO_2 (thin lines). (**A**) Calculated imaginary parts of the dielectric functions (ε_2), which are averaged over three (*x*, *y*, and *z*) polarization vectors. (**B**) Experimental optical absorption spectra of $TiO_{2-x}N_x$ and TiO_2 films.

We prepared $TiO_{2-x}N_x$ films by sputtering the TiO_2 target in an N_2(40%)/Ar gas mixture. After being annealed at 550°C in N_2 gas for 4 hours, the films were crystalline, with features assignable to a mixed structure of the anatase and rutile crystalline phases, as determined by x-ray diffraction (XRD). The $TiO_{2-x}N_x$ films were yellowish and transparent. TiO_2 films were prepared in a similar fashion by sputtering the TiO_2 target in an O_2(20%)/Ar gas mixture and subsequently annealing it at 550°C in O_2 gas for 4 hours. XRD showed that the homogeneous anatase crystalline phase was formed. Optical absorption spectra (Fig. 2B) show that the $TiO_{2-x}N_x$ films noticeably absorb the light at less than 500 nm, whereas the TiO_2 films do not, which is in good agreement with the theoretical results.

Photocatalytic activity was evaluated by measuring decomposition rates of methylene blue as a function of the cutoff wavelength of the optical high-path filters under fluorescent light (Fig. 3A). Substantial photocatalytic ac-

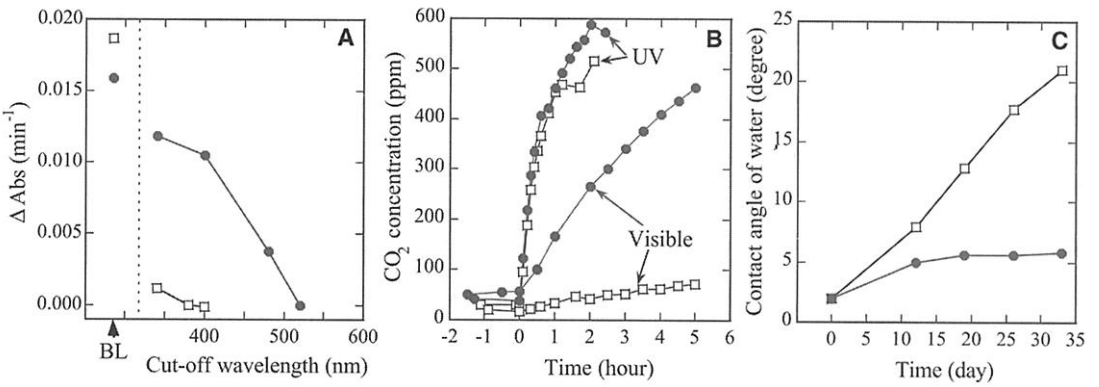

Fig. 3. Photocatalytic properties of $TiO_{2-x}N_x$ samples (solid circles) compared with TiO_2 samples (open squares). (**A**) Decomposition rates [measuring the change in absorption of the reference light (Δabs)] of methylene blue as a function of the cutoff wavelength of the optical high-path filters under fluorescent light with the integrated photon flux of 2.45×10^{-9} einstein (E) s^{-1} cm^{-2} between 350 and 520 nm, compared with the results under BL illumination with the integrated photon flux of 3.51×10^{-9} E s^{-1} cm^{-2} in the UV range. (**B**) CO_2 evolution as a function of irradiation time (light on at zero) during the photodegradation of acetaldehyde gas [with an initial concentration of 485 parts per million (ppm)] under UV irradiation (BL with a peak at 351 nm and the light power of 5.4 mW cm^{-2}) and visible irradiation [fluorescent light cut by the optical high-path filter (SC42, Fuji Photo Film), with a peak intensity at 436 nm and a light power of 0.9 mW cm^{-2}]. (**C**) Contact angles of water as a function of time under interior lighting (with light powers of 28.5 and 159.4 μW cm^{-2} in the UV and visible ranges, respectively). All these light powers were measured by the UV radiometer (UVR-2, TOPCON, Tokyo, Japan) with detectors (UD-36 for the UV range and UD-40 for the visible range).

tivity under 500 nm has been observed in $TiO_{2-x}N_x$ films, and the cutoff wavelength for photocatalytic activity corresponds well with the optical absorption spectra (*21*, *22*). Both $TiO_{2-x}N_x$ and TiO_2 films reveal similar activity under UV light [represented by the results under black light (BL) illumination].

We also evaluated the photodecomposition of gaseous acetaldehyde of $TiO_{2-x}N_x$ powder samples that were prepared by treating anatase TiO_2 powder (ST01, Ishihara Sangyo Kaisha, Osaka, Japan) in the NH_3(67%)/Ar atmosphere at 600°C for 3 hours. The Brunaer-Emmett-Teller surface areas of the $TiO_{2-x}N_x$ and TiO_2 powders were measured as 67 and 270 m^2/g, respectively. Figure 3B shows CO_2 concentrations, evolved as a result of the photodecomposition of acetaldehyde, as a function of irradiation time. The photocatalytic activity of the $TiO_{2-x}N_x$ sample is superior to that of the TiO_2 sample in the visible range of irradiation, whereas both samples yield similar UV activity. We used the photodegradation process of acetaldehyde proposed in (*23*) to estimate quantum yields for the CO_2 evolution, based on the number of incident photons being 0.42% ($TiO_{2-x}N_x$) and 0.14% (TiO_2) at 436 nm, and 3.0% ($TiO_{2-x}N_x$) and 2.6% (TiO_2) at 351 nm.

Our final evaluation of the photocatalytic activity was to measure contact angles of water on the sample films under interior lighting. The so-called photoinduced hydrophilic surface is known as an important application of TiO_2 (*24*, *25*). In this experiment, we used the $TiO_{2-x}N_x$ and TiO_2 films, on which SiO_2 with a nominal thickness of 5 nm was deposited to hold adsorbed water (*25*). The results show an excellent hydrophilic surface of the $SiO_2/TiO_{2-x}N_x$ film, which maintained a contact angle of 6° even after 30 days, in contrast to the SiO_2/TiO_2 film, whose contact angle constantly increased with time (Fig. 3C). As with usual TiO_2 specimens, our $TiO_{2-x}N_x$ samples resisted the attack of acid and alkaline solvents such as H_2SO_4, HCl, H_2O_2, and NaOH at the ambient temperature, and their photocatalytic performance was stable during successive use under 100-W mercury lamp irradiation for more than 3 months.

To investigate N states in $TiO_{2-x}N_x$, we measured N 1*s* core levels with x-ray photoemission spectroscopy (XPS). Three peak structures at the binding energies of 402, 400, and 396 eV were observed for the $TiO_{2-x}N_x$ films (Fig. 4A). We observed similar XPS spectra for the $TiO_{2-x}N_x$ powder samples. The TiO_2 films also included a small amount of N; however, the peak at 396 eV was not observed. Saha *et al.* (*26*) investigated the N 1*s* XPS spectra during the oxidation process of TiN and assigned the peaks as atomic β-N (396 eV) and molecularly chemisorbed γ-N_2 (400 and 402 eV). To elucidate relations to photocatalytic activity systematically, we prepared $TiO_{2-x}N_x$ samples by annealing the TiO_2 powder in the NH_3(67%)/Ar atmosphere at 550° to 600°C. The powder samples were used here, because the reaction temperature and the N concentration in the samples can be easily controlled by changing temperature and time of the NH_3 treatment rather than by changing the sputtering conditions.

Figure 4B shows the decomposition rates of methylene blue under visible light ($\lambda > 400$ nm) as a function of the ratio of the decomposed area in the XPS peak at 396 eV to the total area of N 1*s*. Each powder sample included the total N concentration of about 1 atomic %. An increase of photocatalytic activity with an increase of the component of N with the XPS peak at 396 eV is clearly observed. The decrease in photocatalytic activity observed in the powder sample (e) may be attributed to a change in the crystal structure of the sample caused by the high doping of N in the crystal, although we did not find a noticeable change in XRD. An optimum concentration of N with the XPS peak at 396 eV, which may depend on the preparation process, was found at ~0.25 atomic % (read from Fig. 4B and the total concentrations of N in the samples) or $TiO_{1.9925}N_{0.0075}$. All these results, combined with the theoretical analyses described before (along with Fig. 1), consistently show that the active sites of N for photocatalysis under visible light are the substitutional ones that can be identified with the atomic β-N states peaking at 396 eV in the XPS spectra.

The active wavelength of $TiO_{2-x}N_x$, of less than 500 nm, promises a wide range of applications, as it covers the main peak of the solar irradiation energy beyond Earth's atmosphere (around 460 nm) and an excellent light source peaking at 390 to 420 nm, provided by recently developed light-emitting indium gallium nitride diodes (*27*).

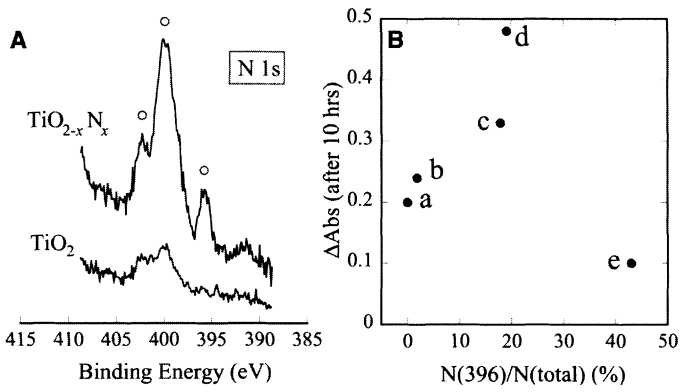

Fig. 4. (**A**) N 1*s* XPS spectra of the (upper lines) $TiO_{2-x}N_x$ and (lower lines) TiO_2 films. (**B**) Decomposition rates (measuring the change in absorption of the reference light after 10 hours) of methylene blue in the aqueous solution under visible light (the same light source as the visible irradiation in Fig. 3B) as a function of the ratio of the decomposed area in the XPS spectra with the peak at 396 eV to the total area of N 1*s*. The total N concentrations for the powder samples were evaluated to be 1.0 atomic %, a; 1.1 atomic %, b; 1.4 atomic %, c; 1.1 atomic %, d; and 1.0 atomic %, e.

References and Notes

1. A. Fujishima, K. Honda, *Nature* **238**, 37 (1972).
2. M. A. Fox, M. T. Dulay, *Chem. Rev.* **93**, 341 (1993).
3. M. R. Hoffmann *et al.*, *Chem. Rev.* **95**, 69 (1995).
4. D. F. Ollis, H. Al-Ekabi, Eds., *Photocatalytic Purification and Treatment of Water and Air* (Elsevier, Amsterdam, 1993).
5. K. I. Hadjiivanov, D. K. Klissurski, *Chem. Soc. Rev.* **25**, 61 (1996).
6. A. Heller, *Acc. Chem. Res.* **28**, 503 (1995).
7. A. Linsebigler, G. Lu, J. T. Yates, *Chem. Rev.* **95**, 735 (1995).
8. A. K. Ghosh, H. P. Maruska, *J. Electrochem. Soc.* **124**, 1516 (1977).
9. W. Choi *et al.*, *J. Phys. Chem.* **98**, 13669 (1994), and references therein.
10. M. Anpo, *Catal. Surv. Jpn.* **1**, 169 (1997).
11. R. G. Breckenridge, W. R. Hosler, *Phys. Rev.* **91**, 793 (1953).
12. D. C. Cronemeyer, *Phys. Rev.* **113**, 1222 (1959).
13. T. Sakata, T. Kawai, in *Energy Resources Through Photochemistry and Catalysis*, M. Grätzel, Ed. (Academic Press, New York, 1983) pp. 332–358.
14. E. Wimmer *et al.*, *Phys. Rev. B* **24**, 864 (1981).
15. H. J. F. Jansen, A. J. Freeman, *Phys. Rev. B* **30**, 561 (1984).
16. L. Hedin, B. I. Lundqvist, *J. Phys. C* **4**, 2064 (1971).
17. The calculations have been done without any geometry optimization for the S doping, because the resulting atomic forces are too large to obtain reasonable positions in the present unit cell (the eight TiO_2 units per cell), giving the positive formation energy of 4.1 eV required for the substitution of S for O, compared with that of 1.6 eV for the substitution of N.
18. We used a rigid shift of the band gaps, 1.14 eV, for both $TiO_{2-x}N_x$ and TiO_2 as in (*19*), assuming that the amount of the band-gap underestimation in LDA would not be affected by doping, because long-range screening properties in $TiO_{2-x}N_x$ are expected to be similar to those in TiO_2.
19. R. Asahi *et al.*, *Phys. Rev. B* **61**, 7459 (2000).
20. M. Jansen, H. P. Letschert, *Nature* **404**, 980 (2000).
21. A possibility of the degradation of methylene blue through the so-called sensitization process in a visible range ($\lambda > 500$ nm) (*22*) can be negligible in the present measurement, because this influence, if any, would have appeared in the results equally at any cutoff wavelength of the high-path filter in the measurement range, which, however, we did not observe.
22. K. Vinodgopal *et al.*, *Environ. Sci. Technol.* **30**, 1660 (1996).
23. I. Sopyan *et al.*, *J. Photochem. Photobiol. A Chem.* **98**, 79 (1996).
24. R. Wang *et al.*, *Nature* **388**, 431 (1997).
25. M. Machida *et al.*, *J. Mater. Sci.* **34**, 2569 (1999).
26. N. C. Saha, H. G. Tompkins, *J. Appl. Phys.* **72**, 3072 (1992).
27. N. M. Johnson *et al.*, *Phys. Today* **53**, 31 (October 2000) and references therein.

28. We thank A. J. Freeman and W. Mannstadt for their continuous support with the FLAPW code, and K. Tanaka and N. Isomura for their experimental support.

28 December 2000; accepted 25 May 2001